Thermochimica Acta 492 (2009) 61–66

Contents lists available at ScienceDirect

Thermochimica Acta

journal homepage: www.elsevier.com/locate/tca

Non-isothermal crystallization of PET/PLA blends

Huipeng Chen [a], Marek Pyda [b], Peggy Cebe [a,*]

[a] Department of Physics and Astronomy, Tufts University, 4 Colby Street, Medford, MA 02155, USA
[b] Department of Chemistry, The University of Technology, Rzeszow, 35959 Rzeszow, Poland

ARTICLE INFO

Article history:
Available online 5 May 2009

Keywords:
Poly(ethylene terephthalate) (PET)
Poly(lactic acid) (PLA)
Blends
Non-isothermal crystallization
Rigid amorphous fraction (RAF)

ABSTRACT

Binary blends of poly(ethylene terephthalate) with poly(lactic acid), PET/PLA, were studied by differential scanning calorimetry and X-ray scattering. The PET/PLA blends, prepared by solution casting, were found to be miscible in the melt over the entire composition range. Both quenched amorphous and semicrystalline blends exhibit a single, composition dependent glass transition temperature. We report the non-isothermal crystallization of (a) PET, with and without the presence of PLA crystals and (b) PLA, with and without the presence of PET crystals. PET can crystallize in all blends, regardless of whether PLA is amorphous or crystalline, and degree of crystallinity of PET decreases as PLA content increases. In contrast, PLA crystallization is strongly affected by the mobility of the PET fraction. When PET is wholly amorphous, PLA can crystallize even in 70/30 blends, albeit weakly. But when PET is crystalline, PLA cannot crystallize when its own content drops below 0.90. These different behaviors may possibly be related to the tendency of each polymer to form constrained chains, *i.e.*, to form the rigid amorphous fraction, or RAF. PET is capable of forming a large amount of RAF, whereas relatively smaller amount of RAF forms in PLA. Like the crystals, the rigid amorphous fraction of one polymer component may inhibit the growth of crystals of the other blend partner.

© 2009 Elsevier B.V. All rights reserved.

1. Introduction

PET is a commercially important engineering thermoplastic with good thermal and mechanical properties, low permeability, and chemical resistance. It is used for example in bottle containers, food packaging, textile fibers, engineering plastics in automobiles, electronics and blood vessel tissue engineering [1–4]. Unlike petroleum-based plastics, biodegradable green plastic PLA is derived from renewable resource, such as corn and starch. PLA is biodegradable polyester with high strength and high modulus. It has various applications in drug delivery, tissue engineering, food packing and bottle containers [5–7]. Recently, PLA bottles have been produced and start to challenge PET bottles especially with the rise in oil prices. PLA bottles have many advantages such as biodegradability, plentiful material source, and lower cost during blow-molding due to its lower glass transition temperature (T_g = 70 °C for PET [8–10] and T_g = 50 °C for PLA [11–13]). However, since PLA is not a good barrier for oxygen and has relatively high cost, the use of PLA bottles is still limited.

Blending is usually used to improve the properties of polymers. Many binary blends of the type A/B with A being either PET or PLA have been produced [14–18]. However, binary blends incorporating both PET and PLA have not yet been investigated. In the present work, the miscibility and thermal properties of PET/PLA blends were studied over a wide composition range from 0% to 100% PLA. In this blend system, both PET, the A component, and PLA, the B component, have the potential to crystallize. Whether they will do so depends upon their relative mass fractions and upon the crystallization conditions, *i.e.*, whether the blends are thermally treated by cooling from the melt state, or by heating from the glassy state.

The crystallization kinetics of a crystallizable polymer with an amorphous polymer in binary polymer blends is different from the kinetics of a crystallizable polymer blended with another crystallizable polymer. In the former case, we expect that the amorphous polymer B component could be diffused from the crystalline growth front of the crystallizing A component. In the latter case, if B is already crystalline, the crystalline fraction would serve as a restriction on the subsequent growth of the crystallizable A partner [18]. However, most prior reports were based on crystallization of the A component with either non-crystalline B component, or crystallized B component. In the present work, we report the non-isothermal crystallization of (a) A component, PET, with and without the presence of PLA crystals, and (b) B component, PLA, with and without the presence of PET crystals.

Even in A/B polymer blends, a three-phase model, comprising crystalline fraction (C), mobile amorphous fraction (MAF), and rigid amorphous fraction (RAF), is proposed to describe the phase structure, instead of using a conventional two-phase model

* Corresponding author.
E-mail address: peggy.cebe@tufts.edu (P. Cebe).

0040-6031/$ – see front matter © 2009 Elsevier B.V. All rights reserved.
doi:10.1016/j.tca.2009.04.023

comprising only crystalline and amorphous fractions. RAF has been found in many well-crystallized polymer blends such as isotactic polystyrene/atactic polystyrene blends [19], polyurethane/poly(methyl methacrylate) blends [20], PET/polystyrene blends [21], polycarbonate/poly(ε-caprolactone) blends [22], poly(ether ether ketone)/polyarylate blends [23], and poly(ether ether ketone)/poly(ether imide) blends [24]. The rigid amorphous fraction (RAF) is the intermediate phase connecting the crystalline phase (C) to the mobile amorphous fraction (MAF); MAF is also called the "conventional" amorphous phase [25–31]. Unlike MAF, the RAF will not undergo relaxation during the conventional glass transition. Furthermore, since the RAF is intimately connected with the crystalline phase, like the crystal fraction, RAF would probably not be diffused from the crystalline growth front and therefore could also restrict the growth of the other blend partner.

PET and PLA have very different abilities to form RAF, even in cases where the crystalline fractions do not differ greatly. In PET, when the crystal fraction, $\phi_C = 0.29$, the RAF fraction, $\phi_{RAF} = 0.49$ [32], giving a total solid fraction, $\phi_S = 0.78$. PLA on the other hand, forms little RAF. In a typical case, PLA with $\phi_C = 0.40$, presents only $\phi_{RAF} = 0.13$ [32], giving a total solid fraction, $\phi_S = 0.53$. If two crystallizable polymers with tendency to form different amounts of RAF are blended, it was our thinking that the confinement ability (RAF-forming ability) of one polymer could affect the subsequent crystallization and crystallinity of its blend partner. Here we explore the non-isothermal crystallization of PET/PLA blends to assess the crystalline fractions, ϕ_C(PET) and ϕ_C(PLA), and, to the extent possible, also the rigid amorphous fractions, ϕ_{RAF}(PET) and ϕ_{RAF}(PLA).

2. Experimental

2.1. Materials

The PET films were obtained from the former Allied Signal Corp. with intrinsic viscosity of 0.92 dl/g, measured in 60/40 phenol/trichloroethylene solution, giving a molecular weight of 25,000 g/mol calculated from the Mark–Houwink equation with $a = 0.640$ and $K = 14 \times 10^{-4}$ dl/g. Poly(lactic acid), PLA-2002D (containing 1.5–2% of D isomer) pellets were obtained from Cargill Dow LLD, NatureWorks LLC, USA. Onset degradation temperature of PLA-2002D is 290 °C. PET and PLA were dissolved separately in hexafluoro-2-propanol (HFIP) to form stock solutions with concentrations of about 10% by weight of polymer. PET/PLA blends were prepared by mixing the stock solutions to achieve the following weight ratios of PET to PLA: 100/0, 90/10, 70/30, 50/50, 30/70, 10/90, and 0/100. Films of the blends were cast from solution, dried in a vacuum oven at 85 °C for several days and then compression-molded above the melting temperature of the PET component and cooled to room temperature to obtain films with uniform thickness about 0.2 mm. Wholly amorphous samples were obtained by quenching the molten samples into liquid nitrogen, and the films were confirmed to be amorphous by X-ray diffraction.

2.2. DSC measurements

DSC studies were carried out using TA instruments temperature modulated DSC (TA Q100). Indium was employed for the temperature and heat flow calibration. The heat capacity was evaluated with respect to sapphire standard. Dry nitrogen gas was purged into the DSC cell with a flow rate of 50 mL/min. The sample mass was kept at about 5–6 mg. Endotherms are presented with downward deflection in our scans.

Crystallinity was determined from the area of the DSC endotherm using 140 J/g as the heat of fusion of 100% crystalline PET [33] and 86 J/g as that of 100% crystalline PLA [33]. The crystallinity

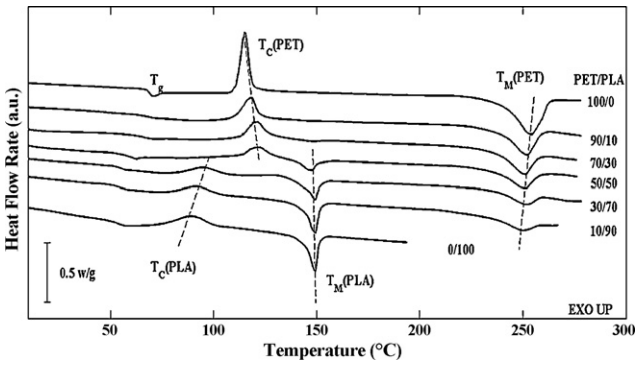

Fig. 1. Heat flow rate vs. temperature of initially wholly amorphous PET/PLA blends during DSC heating at 5 °C/min. Ordinate values have been normalized for total sample mass. Curves are displaced vertically for clarity. The dashed lines are guides to the eye.

can be obtained from:

$$\phi_C = \frac{\Delta H_{(Meas)}}{\Delta H_f} \quad (1)$$

where $\Delta H_{(Meas)}$ is the measured heat of fusion of the semicrystalline polymer and ΔH_f is the heat of fusion of 100% crystalline polymer from the literature.

2.3. Wide angle X-ray scattering

Two-dimensional WAXS patterns of PET/PLA blends were obtained at room temperature on a Bruker AXS from $2\theta = 8$–$30°$ (for θ the half-scattering angle) at wavelength $\lambda = 0.1542$ nm. Scattered intensity was corrected for air background, and the two-dimensional isotropic pattern was converted to a one-dimensional pattern by integrating over a sector.

3. Results and discussion

3.1. Miscibility of PET/PLA blends

Fig. 1 shows the DSC thermograms for wholly amorphous PET/PLA blends, obtained by quenching from the melt. The thermograms show T_g in the range from ~40 °C to 80 °C, followed by crystallization exotherms with peaks marked as T_C(PLA) or T_C(PET). Near 150 °C, the melting of PLA occurs, marked as T_M(PLA) followed by PET melting near 250 °C, marked as T_M(PET). A single melting peak of PET was observed for all the blends. Melting temperature of PET was slightly decreased with an increase of PLA concentration. Similar result was also found in iPS/aPS blends [19,34] and Nylon 6/Silk blends [35]. The PET crystals may become less perfect with PLA addition, or there may be a decrease of the equilibrium melting temperature after blending.

For all blend compositions, the transition temperatures follow the relationship:

$$T_g < T_C(PLA) < T_C(PET) < T_M(PLA) < T_M(PET) \quad (2)$$

All PET/PLA blends exhibit a single glass transition temperature, T_g, which is shown in Fig. 2 as a function of PET composition. T_g of the initially quenched amorphous blends is shown by open circles. The appearance of a single, composition-dependent T_g for the PET/PLA blends indicates that the blends exhibit a homogeneous amorphous phase structure and that PET is completely miscible with PLA over the entire composition range.

Several different relationships have been proposed to describe the dependence of T_g on the composition of miscible polymer blends [19,36–42]. As in our prior work in iPS/aPS blends [19], here

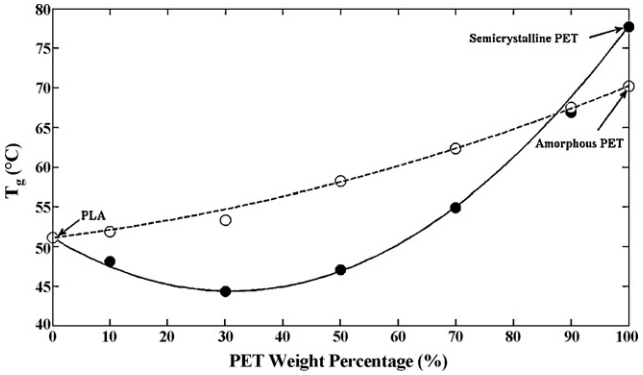

Fig. 2. Glass transition temperature vs. PET content for PET/PLA blends. Open circles—wholly amorphous blends; filled circles—blends crystallized during cooling from the melt at 20 °C/min, containing crystalline PET and amorphous PLA. Solid line is the best fit to the semicrystalline blend data using Eq. (3) with $k = 1.01$ and $p = -70$. Dashed line is the best fit to the wholly amorphous blends data using Eq. (3) with $k = 1.01$ and $p = -10$.

also we use Kwei's equation [39–41] to describe the T_g-composition relationship:

$$T_g = \frac{(W_1 T_{g1} + W_2 T_{g2})}{(W_1 + kW_2)} + pW_1 W_2 \quad (3)$$

where T_g is the glass transition temperature of the blends; T_{g1} and T_{g2} are those of pure components (1 for PET, 2 for PLA); W_1 and W_2 are the weight percent of PET and PLA, respectively; k is an adjustable fitting parameter which can be taken as a quantity characterizing the strength of intermolecular interactions between blend components. The first term on the right-hand side of Eq. (3) is also known as the Gordon–Taylor equation [37]. In the second term on the right-hand side, p represents intermolecular specific interactions in the mixture, accounting for effects of the rearrangements in the neighborhood of the molecular contacts. Some self-association interactions are broken and some inter-association interactions are formed [39,42]. There are a few different forms used for the second term. For example, Tsutsui et al. [38] use $(pW_1W_2/(W_1 + kW_2))$ for the second term. The values of p can be either positive or negative [19,36–42].

Fig. 2 also shows the glass transition temperature vs. PET content for semicrystalline PET/PLA blends after cooling from the melt at 20 °C/min (solid circles). It is confirmed by Fig. 3, and by X-ray analysis, that these blends contain only PET crystals. PLA is unable to crystallize during melt cooling at 20 °C/min, even in the case of the PLA homopolymer (blend 0/100). Crystallized blends

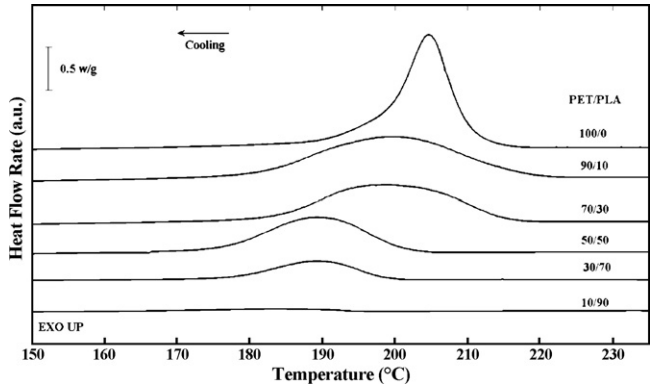

Fig. 3. Heat flow rate vs. temperature of PET/PLA blends during cooling from the melt at 20 °C/min. Ordinate values are normalized for total sample mass. Curves are displaced vertically for clarity. Exothermic peaks arise solely from crystallization of PET.

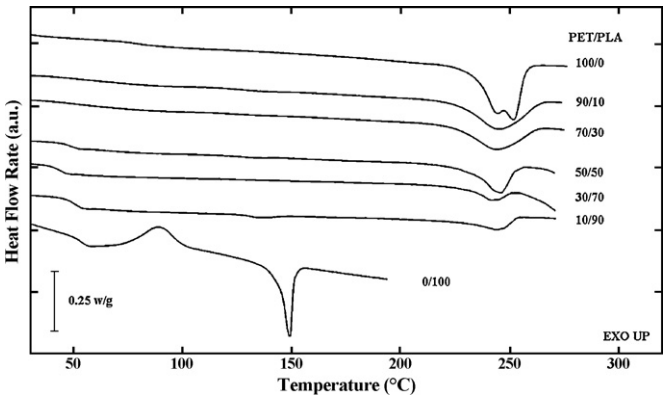

Fig. 4. Heat flow rate vs. temperature of PET/PLA blends during heating at 5 °C/min after cooling from the melt at 20 °C/min. Ordinate values are normalized for total sample mass. Curves are displaced vertically for clarity.

in the compositions we investigated generally have a decrease of T_g compared to the quenched amorphous samples except for homopolymer PET. Fig. 2 shows the glass transition temperature vs. PET content for crystalline PET/PLA blends, crystallized during cooling from the melt at 20 °C/min (filled circles). T_g's of the crystalline PET/PLA blends can be fitted by Eq. (3) with $k = 1.01$ and $p = -70$. For the quenched amorphous PET/PLA blends, the fitting parameters k and p are 1.01 and −10, respectively. The large negative value of p indicates a strong intermolecular interaction between PET and PLA [19,39–42] regardless of whether the sample is amorphous or crystalline, and crystalline blends (with PET crystalline/PLA amorphous) show much stronger intermolecular interaction than wholly amorphous blends.

3.2. Cold crystallization of PLA in the presence of amorphous PET

In Fig. 1, during heating from the glassy wholly amorphous state homopolymer PET shows a non-isothermal cold crystallization peak at about T_C(PET) = 110 °C and homopolymer PLA shows its crystallization peak at T_C(PLA) = 90 °C, 20 degrees lower than PET. For PET/PLA blends, PLA crystallized earlier than PET during heating. The crystallization temperature of PLA shifts to higher temperature with an increase of amorphous PET concentration (shown by dashed lines in Fig. 1) and crystallization of PLA is not observable as an exothermic peak when the weight fraction of PET was higher than 0.30. Meanwhile, crystallization of PET also shifted to higher temperature with an increase of PLA composition and cold crystallization of PET during heating was still possible even in the 10/90 blends. In blend 10/90, no clear exotherm can be seen for PET, but its crystallization during heating is confirmed by appearance of the endotherm at T_M(PET) ~250 °C.

3.3. Melt crystallization of PET in the presence of amorphous PLA

Fig. 3 shows the DSC thermograms for semicrystalline PET/PLA blends during cooling from the melt at 20 °C/min. Crystallization temperature of PET, T_{MC}(PET) (melt crystallization) shifts to lower temperature and the exotherm broadens, with the increased content of amorphous PLA. Since T_C(PLA) < T_C(PET), PET crystallizes from the melt in the presence of wholly amorphous, molten PLA. After cooling from the melt to room temperature, the PLA component in all the blends was still fully amorphous. That fact is confirmed by both DSC results in Fig. 4 and X-ray results in Fig. 5. In Fig. 5, no crystal peaks of PLA were observed for the blends.

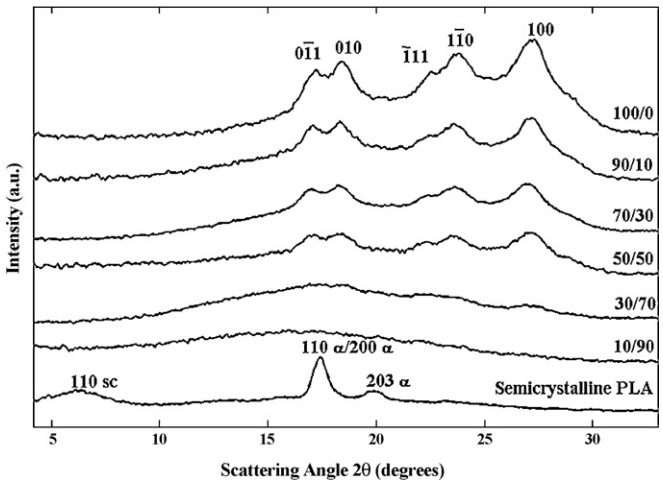

Fig. 5. WAXS intensity vs. scattering angle, 2θ (for $\lambda = 0.154$ nm), at room temperature for PET/PLA blends non-isothermally crystallized by cooling from the melt at 20 °C/min with compositions as marked. In the blend samples all the crystal peaks are related to PET crystals. The lower curve shows crystalline PLA for comparison. Miller indices are marked above the homopolymer curves. For semicrystalline PLA, the Miller indices refer to orthorhombic crystal structure (alpha phase) and stereo-complex crystals (sc) found in mixed isomer systems of PLLA with PDLA [43].

3.4. Cold crystallization of PLA in presence of crystallized PET

Fig. 4 shows DSC thermograms for PET/PLA blends during heating at 5 °C/min after cooling from the melt at 20 °C/min. As mentioned above, the blends were confirmed to contain crystalline PET and amorphous PLA. For PLA homopolymer, an exothermic peak due to the crystallization of PLA was observed. For the blends, only for the PET/PLA 10/90 was a very tiny melting peak of PLA observed, caused by melting of PLA crystals formed during the heating. However, when the content of PET increased to 0.30, and the PET was already previously crystallized, then the crystallization of PLA was totally inhibited.

The absence of crystallization of the PLA is not simply due to the diluting effect of blending with PET, since cold crystallization of PLA in the presence of *amorphous* PET occurs readily even in PET/PLA 70/30. The modified Turnbull–Fisher equation which represents the spherulitic growth rate, G, in polymer blends is expressed by [44–47]:

$$G = G_0 \nu_2 \exp\left[\frac{U}{k_B(T_C - T_\infty)} - \frac{K_g T_M^0}{f T_C \Delta T} + \frac{0.2 T_M^0 \ln \nu_2}{f \Delta T}\right] \quad (4)$$

where G_0 is constant; ν_2 is the volume fraction of the respective polymer; U is the activation energy for molecular transport; T_C is the selected crystallization temperature; k_B is the Boltzmann constant; T_∞ is the temperature below which chain transport is impossible; T_M^0 is the equilibrium melting temperature of the respective polymer; ΔT is the degree of supercooling; f is a correction factor and equals $2T_C/(T_C + T_M^0)$; and K_g is usually regarded as a constant [44], related to the lamellar lateral and end surface free energies. The crystallization of the PET component is suggested to form a mobility restricted region which reduces the growth of PLA crystals, affecting the activation energy for cold crystallization, U, in Eq. (4).

In Fig. 4, homopolymer PET exhibits two endothermic melting peaks. The explanation for the multiple melting peaks of PET is a melting–recrystallization–remelting model, in which the lower endotherm (occurring at lower temperature) is due to the melting of original crystals and the higher temperature endotherm is due to the melting of crystals that recrystallized during heating after melting of the original crystals [48]. With the addition of any amount of PLA, only one broad melting peak was observed, and the upper melting endotherm is not distinguishable.

3.5. Cold crystallization of PET in the presence of crystallized PLA

As discussed above, and shown in Fig. 1, for PET/PLA blends, the PLA component crystallized at a lower temperature than PET during heating. Therefore, subsequent crystallization of PET occurs in the presence of already-crystallized PLA from compositions 70/30 to 10/90. Crystallization peak temperature of PET shifts to higher values as PLA content increases. This suggests that an increase of chain mobility (brought by higher temperature) is needed in order for PET to crystallize as the PLA content increases.

Whereas the PET component could cold crystallize in the presence of crystalline PLA up to 0.90 PLA fraction (see Fig. 1), the PLA component was unable to cold crystallize in the presence of crystalline PET in blends with greater than 0.10 PET fraction (see Figs. 4 and 5). We speculate that this is might be related to the different abilities of PLA and PET to form the rigid amorphous fraction: RAF in PET can be very large compared with PLA [32]. Like the crystals, the rigid amorphous fraction of one polymer may block the growth of crystals of the other blend partner. To determine the degree of crystallinity, ϕ_C(PET) and ϕ_C(PLA), of the blends, Eq. (1) was used, and these results are listed in Table 1. PET can crystallize in all blends, regardless of whether PLA is amorphous or crystalline, and ϕ_C(PET) decreases as PLA content increases. In contrast, PLA crystallinity is strongly affected by the mobility of the PET fraction. When PET is wholly amorphous (Table 1, row 3), PLA can crystallize even in 70/30 blends (albeit weakly: ϕ_C(PLA) = 0.01). But when PET is crystalline (Table 1, row 5), PLA cannot crystallize when its own content drops below 0.90. In 10/90, ϕ_C(PLA) has already decreased to 0.02, down from 0.25 in homopolymer PLA.

As mentioned above, both PLA and PET can cold crystallize in the presence of an amorphous blend partner. However, in the presence of *crystalline* polymer, crystallization rates of PET and PLA are extremely different. At the scanning rate used in this study (5 °C/min), PLA cannot crystallize when its own content drops below 0.90, while PET can crystallize in all blends. So the different crystal growth rates are most likely due to the restrictions caused by prior crystallization of the blend partner and not simply due to the diluent effect of blending. This leads us to consider the role of the crystals. As mentioned above, the crystalline fraction would serve as a restriction on the subsequent growth of the other polymer. As shown in Table 1, for PET/PLA 50/50 blends, before the cold crystallization of PET, the crystallinity of PLA is 0.10; before the cold crystallization of PLA, the crystallinity of PET is 0.14. The crystalline fractions are very similar in these two systems, but PET can easily

Table 1
Crystallinity of PET and PLA in PET/PLA blends.

PET/PLA	100/0	90/10	70/30	50/50	30/70	10/90	0/100
ϕ_C(PET)[a](±.01)	0.30	0.27	0.23	0.17	0.10	0.04	0
ϕ_C(PLA)[b](±.01)	0	0	0.01	0.10	0.18	0.22	0.25
ϕ_C(PET)[c](±.01)	0.31	0.25	0.20	0.14	0.08	0.03	0
ϕ_C(PLA)[d](±.01)	0	0	0	0	0	0.02	0.25

[a] Crystallinity of PET after non-isothermal crystallization of PET during heating of wholly amorphous samples and determined from heat of fusion of PET in Fig. 1 using Eq. (1).

[b] Crystallinity of PLA after non-isothermal crystallization of PLA during heating of wholly amorphous samples and determined from heat of fusion of PLA in Fig. 1 using Eq. (1).

[c] Crystallinity of PET after non-isothermal crystallization of PET during cooling from the melt and determined from heat of crystallization of PET in Fig. 3 using Eq. (1).

[d] Crystallinity of PLA after non-isothermal crystallization of PLA during heating after cooling from the melt and determined from heat of fusion of PLA in Fig. 4 using Eq. (1).

Table 2
Mobile amorphous, rigid amorphous and solid fractions of PET after non-isothermal crystallization of PET during cooling from the melt.

PET/PLA	100/0	90/10	70/30	50/50	30/70	10/90	0/100
ϕ_{MA} (±.01)	0.26	0.20	0.28	0.54	0.75	0.90	100
ϕ_{RAF} (±.01)	0.43	0.55	0.52	0.32	0.17	0.07	0
ϕ_S (±.01)	0.74	0.80	0.72	0.46	0.25	0.10	0

crystallize in the 50/50 blend whereas PLA cannot. This led us to consider, in the next section, the possible effect of the rigid amorphous fraction on non-isothermal crystallization in PET/PLA blends, since the RAF contents are greatly different between PET and PLA even in samples with about the same crystallinity.

3.6. Rigid amorphous fraction in PET/PLA blends

In this section, we consider the determination of the RAF that exists in the already-crystallized blend partner, before the other partner crystallizes. Two situations must be distinguished: (1) calculation is made of the RAF content of PET prior to PLA crystallization, but, (2) we cannot calculate directly the RAF content of PLA prior to PET crystallization, and therefore it must be estimated. We consider these cases separately below.

1. For non-isothermal cold crystallization of PLA in the presence of crystallized PET, the RAF content of the PET can be obtained by the following method. First, the mobile amorphous fraction, ϕ_{MA}, in the PET/PLA blends can be obtained using:

$$\phi_{MA} = \frac{\Delta C_P^{Meas}(T_g)}{[\Delta C_P^{PET}(T_g)W^{PET} + \Delta C_P^{PLA}(T_g)W^{PLA}]} \quad (5)$$

where $\Delta C_P^{Meas}(T_g)$ is the measured heat capacity step at T_g; ΔC_P^{PET} and ΔC_P^{PLA} are the heat capacity steps at T_g for 100% amorphous PET and 100% amorphous PLA, respectively. As shown in Fig. 1, T_g is different for different blends and ΔC_P for 100% amorphous sample is obtained from heat capacity difference between 100% solid and 100% liquid at the selected T_g. Therefore, different T_g will give different heat capacity step for the 100% amorphous sample. The heat capacity of 100% solid and 100% liquid states for PET and PLA are taken from the ATHAS data bank [33]. Then the RAF content of the PET, ϕ_{RAF}, and the total solid fraction, ϕ_S, can be obtained using:

$$\phi_{RAF} = 1 - \phi_{MA} - \phi_C(\text{PET}) \quad (6a)$$

$$\phi_S = 1 - \phi_{MA} \quad (6b)$$

where ϕ_C(PET) is the crystallinity of PET after non-isothermal melt crystallization during cooling. The results of ϕ_{RAF}, ϕ_{MA}, and ϕ_S are shown in Table 2.

2. On the other hand, for cold crystallization of PET in the presence of already-crystallized PLA, it is impossible to use the above calculation to determine the RAF content of the PLA. The reason is that PET cold crystallizes immediately after, or even along with, the crystallization of PLA. Therefore, we use prior results for PLA samples of known crystallinity [32] to help estimate the RAF content of PLA. Under the assumption that the crystalline fraction and rigid amorphous faction have a linear relationship to one another, we can estimate the RAF of PLA. For example, as mentioned in Section 1, in a PLA sample with $\phi_C = 0.40$, the authors report $\phi_{RAF} = 0.13$ [32]. This result is for homopolymer PLA, and gives a ratio of $\phi_C/\phi_{RAF} = 3.1$.

For PLA in blends, the relationship of crystal fraction to rigid amorphous fraction should be investigated. The PET/PLA 50/50 blend was selected for a special thermal treatment. Quenched

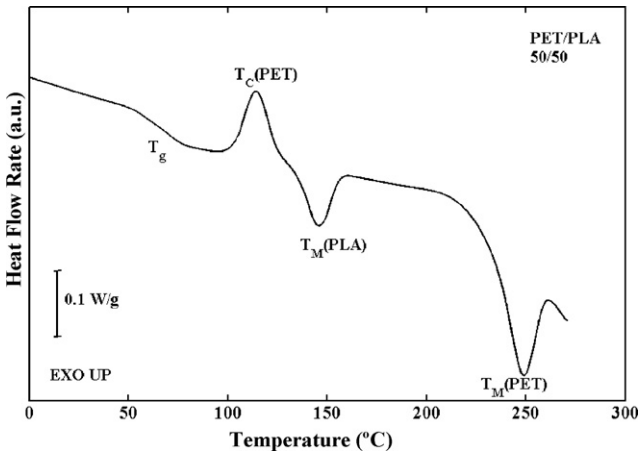

Fig. 6. Heat flow rate vs. temperature of PET/PLA blends during heating at 5 °C/min after cold crystallization at 87 °C for 1 h from initially fully amorphous sample. Ordinate values are normalized for total sample mass.

PET/PLA 50/50 blend (fully amorphous) was cold crystallized at 87 °C for 1 h to let PLA crystallize and then the blend was cooled to −20 °C and reheated at 5 °C/min using DSC. Fig. 6 shows the DSC scan of this blend during reheating. ϕ_C, ϕ_{MA}, and ϕ_{RAF} were determined using Eqs. (1), (5), and (6), respectively. We found the PLA RAF component of this specially treated sample was $\phi_{RAF} = 0.04$ when the crystallinity of PLA was $\phi_C = 0.17$, giving a ratio of $\phi_C/\phi_{RAF} = 4.2$. In this test of the 50/50 PET/PLA blend, and in Ref. [32], the RAF fraction of PLA is small (never greater than 0.04), and the crystal fraction is about 3.1–4.2 times greater than the RAF fraction.

With this insight, we use Ref. [32] to help us estimate the RAF content of non-isothermally cold crystallized PLA. For the 50/50 blend, we estimate the RAF as follows. In PET/PLA 50/50 sample, with PLA cold crystallized during heating from the wholly amorphous state (*i.e.*, there are no PET crystals) $\phi_C = 0.10$ as shown in Table 1, before the start of cold crystallization of PET, and under the assumption that crystallization of PLA is completed before the start of crystallization of PET. The solid fraction in PET/PLA 50/50 is about 0.13, from $\phi_S = \phi_C + \phi_{RAF} = 0.10 + 0.03$. (The ϕ_{RAF} was estimated by linear proportion from the RAF and corresponding crystallinity measured in Ref. [32].) So before the start of cold crystallization of PET, there is about 0.13 solid fraction in PET/PLA 50/50, of which about 0.03 comes from RAF and 0.10 from PLA crystals. ϕ_C(PLA) is less than 0.23 in all the compositions we studied and if the ratio $\phi_C/\phi_{RAF} = 4.2$ had been used rather than 3.1, it would increase the ϕ_{RAF} by at most 0.02. This variation has been incorporated into the error range of the symbols in Fig. 7.

The solid fraction of the PET/PLA 50/50 blends having PET crystallized is about three times greater than the solid fraction in the PET/PLA 50/50 blends having PLA crystallized (*i.e.*, $\phi_S = 0.46$ in PET/PLA 50/50 with crystalline PET, and $\phi_S = 0.13$ in PET/PLA 50/50 with crystalline PLA). Note that the crystallinity values are close for these two systems ($\phi_C = 0.10$ in PET/PLA 50/50 with crystalline PLA, and $\phi_C = 0.14$ in PET/PLA 50/50 with crystalline PET) whereas the solid fractions differ greatly. Fig. 7 shows the crystalline and rigid amorphous fractions vs. the weight content of the other component before the crystallization of the other component. ϕ_C(PET) and ϕ_S(PET) are the crystal and solid fractions, respectively, in PET/PLA blends before the cold crystallization of PLA. ϕ_C(PLA) and ϕ_S(PLA) are the crystal and solid fractions, respectively, in PET/PLA blends before the cold crystallization of PET. For ϕ_C(PET) and ϕ_S(PET), the weight content of the other component is the weight content of PLA in PET/PLA blends; for ϕ_C(PLA) and ϕ_S(PLA), the weight content of the other component is the weight content of PET in PET/PLA blends. ϕ_C(PLA) and ϕ_C(PET) are very close before the crystalliza-

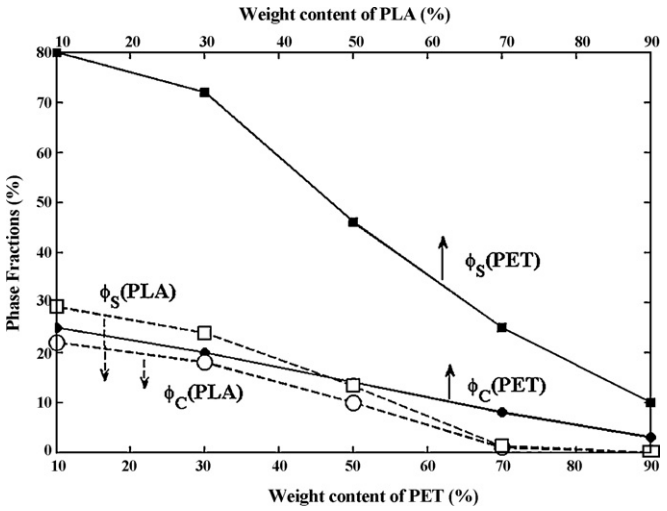

Fig. 7. Phase fractions vs. weight content of the one component before the crystallization of the other component. ϕ_C(PET) (filled square) and ϕ_S(PET) (filled circle) are the crystal and solid fractions, respectively, in PET/PLA blends before the cold crystallization of PLA. ϕ_C(PLA) (open square) and ϕ_S(PLA) (open circle) are the crystal and solid fractions, respectively, in PET/PLA blends before the cold crystallization of PET. For ϕ_C(PET) and ϕ_S(PET), the weight content of the other component is the weight content of PLA in PET/PLA blends (upper abscissa); for ϕ_C(PLA) and ϕ_S(PLA), the weight content of the other component is the weight content of PET in PET/PLA blends (lower abscissa). The lines are guides to the eye.

tion of PET and PLA. However, ϕ_S(PET) is several times greater than ϕ_S(PLA) before the crystallization of the other component. The extreme difference in spherulitic growth rates should result from the *solid fraction* rather than simply from the crystalline fraction. Thus, in A/B polymer blends, it is better to use the solid fraction rather than the crystalline fraction of the A or B polymer to characterize the impact of the crystallization of one partner upon the other partner's ability to crystallize. The impact can be seen in the PET/PLA blends. PLA could easily cold crystallize in 50/50 blends with PET un-crystallized as shown in Fig. 1, but cannot crystallize in the presence of the very large PET solid fraction.

4. Conclusions

Blends of PET/PLA prepared by solution casting were studied by differential scanning calorimetry and X-ray scattering and found to be miscible in the melt over the entire composition range. Both quenched amorphous and semicrystalline blends exhibit a single, composition dependent glass transition temperature. PET can crystallize in all blends, regardless of whether PLA is amorphous or crystalline, and degree of crystallinity of PET decreases as PLA content increases. In contrast, PLA crystallization is strongly affected by the mobility of the PET fraction. When PET is wholly amorphous, PLA can crystallize even in 70/30 blends, albeit weakly. But when PET is crystalline, PLA cannot crystallize when its own content drops below 0.90. This might be related to the different abilities of PLA and PET to form the rigid amorphous fraction: RAF in PET can be very large compared with PLA, leading to a very large solid fraction once PET has crystallized. Like the crystals, the rigid amorphous fraction of one polymer may block the growth of crystals of the other blend partner. Further work is underway to develop the calorimetric approaches needed directly to quantify RAF in binary blends.

Acknowledgements

The authors thank the National Science Foundation for support of this work through the Polymers Program of the Division of Materials Research under DMR-0602473 and the MRI Program under DMR-0520655 for thermal analysis instrumentation. HC and PC thank Prof. Marek Pyda for providing PLA-2002D.

References

[1] H.L. Safa, F. Bourelle, Packag. Technol. Sci. 12 (1999) 67.
[2] K. Parikh, K. Cattanach, R. Rao, D.S. Suh, A.M. Wu, S.K. Manohar, Sens. Actuators B 113 (2006) 55.
[3] M. Wu, L.L. Shaw, Int. J. Hydrogen Energy 30 (2005) 373.
[4] M. Wu, L.L. Shaw, J. Power Sources 136 (2004) 37.
[5] Y. Shikinami, M. Okuno, Biomaterials 22 (2001) 3197.
[6] S.M. Li, M. Vert, Macromolecules 36 (2003) 8008.
[7] H. Tsuji, Biomaterials 24 (2003) 537.
[8] P. Slobodian, J. Therm. Anal. Calorim. 94 (2008) 545.
[9] H.P. Chen, P. Cebe, Macromolecules 42 (2009) 288.
[10] J.E.K. Schawe, Thermochim. Acta 461 (2007) 145.
[11] M. Pyda, R.C. Bopp, B. Wunderlich, J. Chem. Thermodyn. 36 (2004) 731.
[12] M. Pyda, B. Wunderlich, Macromolecules 38 (2005) 10472.
[13] E. Zuza, J.M. Ugartemendia, A. Lopez, E. Meaurio, A. Lejardi, J.R. Sarasua, Polymer 49 (2008) 4427.
[14] G. Georgiev, P. Cebe, M. Capel, J. Mater. Sci. 40 (2005) 1141.
[15] P.S.C. Pereira, L.C. Mendes, M.L. Dias, L. Sirelli, J. Therm. Anal. Calorim. 87 (2007) 667.
[16] M. Shibata, N. Teramoto, Y. Inoue, Polymer 48 (2007) 2768.
[17] J.M. Zhang, K. Tashiro, H. Tsuji, A.J. Domb, Macromolecules 40 (2007) 1049.
[18] M.H. Rahman, A.K. Nandi, Polymer 43 (2002) 6863.
[19] H.P. Chen, H. Xu, P. Cebe, Polymer 48 (2007) 6404.
[20] P.S.O. Patricio, J.A. de Sales, G.G. Silva, D. Windmoller, J.C. Machado, J. Membr. Sci. 271 (2006) 177.
[21] R.J. Schexnaydre, B.S. Mitchell, J. Polym. Sci. Part B: Polym. Phys. 46 (2008) 1348.
[22] E. Laredo, M. Grimau, P. Barriola, A. Bello, A.J. Muller, Polymer 46 (2005) 6532.
[23] Y.S. Chun, Y.S. Han, J.C. Hyun, W.N. Kim, Polymer 41 (2000) 8717.
[24] H.S. Lee, W.N. Kim, Polymer 38 (1997) 2657.
[25] J. Park, M. Pyda, B. Wunderlich, Macromolecules 36 (2004) 495.
[26] H. Chen, P. Cebe, J. Therm. Anal. Calorim. 89 (2007) 417.
[27] H. Xu, B.S. Ince, P. Cebe, J. Polym. Sci. Part B: Polym. Phys. 41 (2003) 3026.
[28] P.P. Huo, P. Cebe, Macromolecules 25 (1992) 902.
[29] C. Schick, A. Wurm, A. Mohammed, Thermochim. Acta 396 (2003) 119.
[30] C. Schick, A. Wurm, A. Mohammed, Colloid Polym. Sci. 279 (2001) 800.
[31] J. Ma, A. Habenschuss, B. Wunderlich, Thermochim. Acta 471 (2008) 90.
[32] M. Arnoult, E. Dargent, J.F. Mano, Polymer 48 (2007) 1012.
[33] M. Pyda, ATHAS data bank, http://athas.prz.rzeszow.pl/, 2008.
[34] J.P. Runt, Macromolecules 14 (1981) 420.
[35] H. Chen, X. Hu, P. Cebe, J. Therm. Anal. Calorim. 93 (2008) 201.
[36] T.G. Fox, Bull. Am. Phys. Soc. 1 (1956) 123.
[37] M. Gordon, J.S. Taylor, J. Appl. Chem. 2 (1952) 496.
[38] T. Tsutsui, H. Nakano, R. Tanaka, T. Tanaka, Kobunshi Ronbunshu 35 (1978) 517.
[39] T.K. Kwei, Macromolecules 20 (1987) 174.
[40] J. Pennacchia, E. Pearce, T.K. Kwei, Macromolecules 19 (1986) 973.
[41] S. Zheng, Y. Mi, Polymer 44 (2003) 1067.
[42] E. Meaurio, E. Zuza, J.R. Sarasua, Macromolecules 38 (2005) 1207.
[43] M. Fujita, T. Sawayanagi, H. Abe, T. Tanaka, T. Iwata, K. Ito, T. Fujisawa, M. Maeda, Macromolecules 41 (2008) 2852.
[44] J. Boon, J.M. Azcue, J. Polym, Sci. Part A-2: Polym. Phys. 6 (1968) 885.
[45] T. Ikehare, H. Kurihara, Z.B. Qiu, T. Nishi, Macromolecules 40 (2007) 8726.
[46] A.T. Lorenzo, M.L. Arnal, A.J. Muller, A. Boschetti-de-Fierro, Macromolecules 40 (2007) 5023.
[47] T. Ikehara, H. Kurihara, T. Kataoka, J. Polym, Sci. Part B: Polym. Phys. 47 (2009) 539.
[48] A.A. Minakov, D.A. Mordvintsev, C. Schick, Polymer 45 (2004) 3755.